Received: 12 November 2020 | Revised: 12 December 2020 | Accepted: 18 December 2020

DOI: 10.1002/qua.26603

FULL PAPER

International Journal of QUANTUM CHEMISTRY WILEY

Toward a two-dimensional NbS_2-based electrode for lithium–ion batteries

Armando S. de Rezende Neto[1,2] | Leandro Seixas[1,2]

[1]MackGraphe—Graphene and Nanomaterials Research Center, Mackenzie Presbyterian University, São Paulo, Brazil

[2]School of Engineering, Mackenzie Presbyterian University, São Paulo, Brazil

Correspondence
Leandro Seixas, School of Engineering, Mackenzie Presbyterian University, Rua da Consolação 896, São Paulo 01302-907, SP, Brazil.
Email: leandro.seixas@mackenzie.br

Funding information
Conselho Nacional de Desenvolvimento Científico e Tecnológico, Grant/Award Numbers: 306422/2017-4, 40825/2018-5; Fundação de Amparo à Pesquisa do Estado de São Paulo, Grant/Award Number: 2017/00486-1

Abstract

The discovery and design of materials for Li–ion batteries are essential for increasing battery energy storage capacity and lifetime, enhancing security, and shortening charging time. Recently, novel two-dimensional materials have been investigated for application in battery components, including the anode. The limiting factors in the development of these materials are their low structural stability upon Li^+ adsorption, propensity to form Li dendrites, and slow diffusion of Li^+ ions. In this study, based on density functional theory calculations, we show that the two-dimensional material 2H-NbS_2 has outstanding physical properties for application in Li–ion batteries, including high structural stability with Li^+ adsorption and ultrafast Li diffusion at room temperature. These results highlight the promise of 2H-NbS_2 as an appealing material for Li–ion batteries.

KEYWORDS
2d materials, density functional theory, li-ion battery, lithium adsorption, lithium diffusion

1 | INTRODUCTION

Lithium–ion batteries (LIBs) [1, 2] are energy storage devices with wide commercial applications in portable electronics, automobiles, and building facilities. LIBs have great advantages over other energy storage devices due to their high capacity to store energy in a reversible way, long lifetimes, and high power densities. Due to the great contribution of LIBs to modern life, the 2019 Nobel Prize in chemistry was awarded for the development of LIBs [3]. However, the development of LIBs with greater energy storage, longer lifetimes, and faster recharging demands new materials for LIB components. Current anode (negative electrode) materials are based on graphite. Novel lamellar materials have been studied in recent years to replace graphite as the anode material. Some recently published works have focused on two-dimensional (2D) materials such as black phosphorus [4], group IV monochalcogenides [5], MXenes [6], and transition metal dichalcogenides (TMDs) [7–9]. 2H-MoS_2 has been extensively studied for application in battery electrodes [7, 8, 10, 11]. In 2H-MoS_2, a phase transition from the 2H phase to the 1T′ phase occurs upon lithiation. This phase transition increases the electrical conductivity of MoS_2 but also results in a loss of stored energy [12]. 2H-MoS_2 is a semiconductor, making it difficult to apply this material as an electrode. The bandgap of bulk 2H-MoS_2 is 1.29 eV (indirect), while that of 2H-MoS_2 monolayer is 1.90 eV (direct) [13]. These issues related to the phase transition and electrical properties can be resolved by using other TMDs. Recently, transition metal (Fe, Co, or Ni)-doped NbS_2 was synthesized and applied as the LIB anode [14]. Also, recently the two-dimensional $NbS2_2$ was studied for applications in Na–ion batteries [15], with very promising results for high energy storage devices. However, physical properties of NbS_2-based materials as (2H-to-1T) phase stability and Li diffusivity needs more clarifications.

In this study, we conducted ab initio calculations to investigate the electronic and structural properties of TMD NbS_2 polytype monolayer (2H and 1T phases) with Li^+ adsorption. The electrical properties of the material along with the adsorption and diffusion of Li^+ were studied to evaluate the applicability of using this 2D material in novel battery technologies.

Novel 2D materials with potential applications in LIBs must meet the following requirements: (i) high structural stability with Li adsorption; (ii) low propensity to form Li dendrites; (iii) high electrical conductivity; and (iv) high ionic conductivity (fast Li diffusion). The results of this study demonstrate that 2H-NbS_2 satisfies these criteria for application as a high-performance anode material.

2 | METHODS

All electronic structure calculations were carried out using density functional theory (DFT) [16, 17] implemented in the SIESTA code [18]. Electron–ion interactions were based on norm-conserved pseudopotentials parameterized by Troullier–Martins pseudopotentials [19]. Exchange–correlation interactions were based on the generalized gradient approximation with Perdew–Burke–Ernzerhof parameterization [20]. We used mesh cutoffs of 350 Ry for structural relaxation and electronic properties and 500 Ry for Bader analysis. The basis functions were based on double-ζ functions with polarization orbitals and an energy shift of 30 meV. The Brillouin zone was sampled using a Monkhorst–Pack mesh with dimensions of $12 \times 12 \times 1$ [21]. For density of states calculations, we used a $100 \times 100 \times 1$ Monkhorst–Pack mesh. All geometries were relaxed until the forces were smaller than 0.01 eV/Å. For transition state (TS) theory, we use the nudged elastic band (NEB) method [22] implemented in the ASE framework [23].

3 | RESULTS AND DISCUSSION

3.1 | Lithium adsorption and dendrites

Based on a model with disordered stacking of NbS_2 layers, the NbS_2 monolayer can be used for the study of battery electrodes. Figure 1 shows the top and side views of the 2H and 1T phases of NbS_2. The sites for Li adsorption above the metal (Nb), above the chalcogen (S), and at the center of the hollow hexagon are labeled as M, X, and h, respectively. For the 1T phase, each hexagon center has an S atom on the opposite face.

We calculated the Li adsorption energy as

$$\Delta E_{ads} = \frac{E_{tot}[Li_xNbS_2] - E_{tot}[NbS_2] - xE_{tot}[Li]}{x}, \quad (1)$$

where x is the number of Li atoms in the unit cell, and $E_{tot}[Li]$ is the total energy of an isolated Li atom. All adsorption energies were negative, indicating strong affinity between Li ions and NbS_2. These adsorption energies were smaller than the cohesive energy of Li (u_{Li} = −1.40 eV),

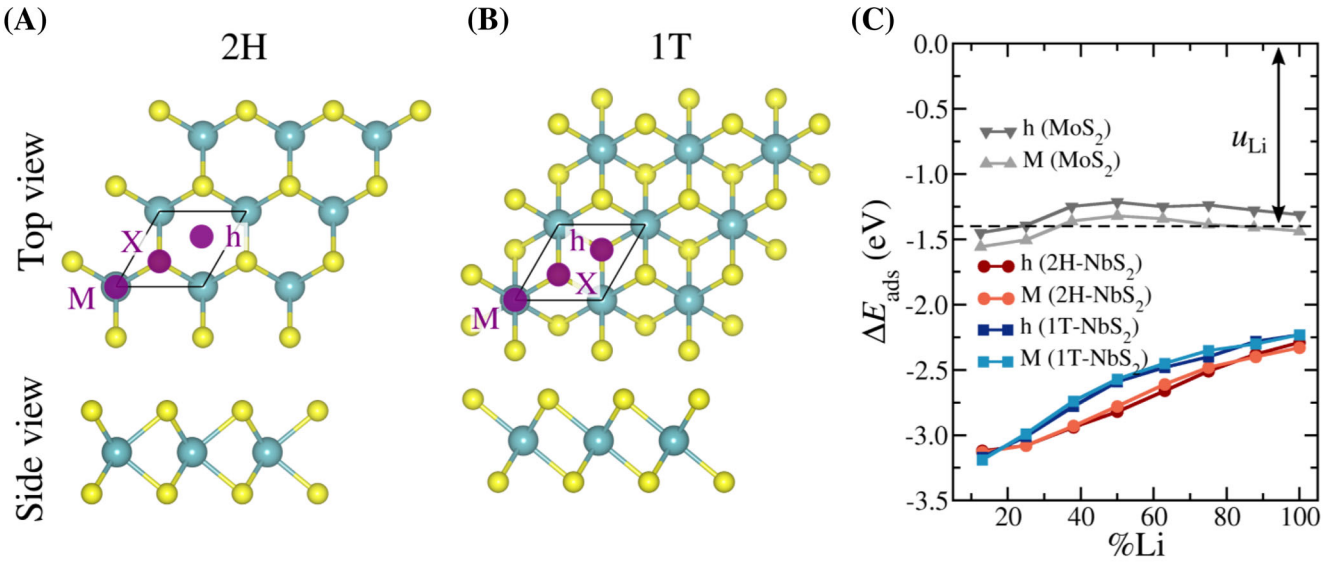

FIGURE 1 Lithium adsorption. Ball-and-stick representations of the (A) 2H and (B) 1T phases of NbS_2. (C) Lithium adsorption energy as function of Li coverage for different sites and phases. Li adsorption on MoS_2 is shown for comparison with NbS_2. The cohesive energy of Li (u_{Li}) is shown as a reference for Li dendrite formation

indicating low propensity to form Li dendrites in the NbS_2 electrode. If the adsorption energies are greater than the cohesive energy of Li, Li dendrites (or Li clusters) will tend to form on the electrode [24, 25]. During the charging process, these Li dendrites can penetrate the separator and cause serious safety problems for the LIB, including fire and explosion [26].

The adsorption energies of Li^+ on NbS_2 were much higher than those on 2H-MoS_2. The Li^+ adsorption energies (ΔE_{ads}) on the M and h sites were considerably smaller than those on the S site ($\Delta E_{ads} \approx -1.6$ eV), and the energies were similar between the two phases. The difference between the Li adsorption energies on the M and h sites for NbS_2 and MoS_2 are shown in Figure S1. These sites can be considered more stable and equivalent for Li adsorption. Lower concentrations of Li^+ correspond to stronger adsorption energies. At higher concentrations, the adsorption energies can increase by ~1.0 eV. NbS_2 provides stable Li^+ adsorption in the entire stoichiometric range, which is a desirable feature in a LIB electrode.

3.2 | Structural stability

One criteria of new materials for battery electrodes is structural stability. That is, the material must maintain its crystalline structure with minimal structural changes when hosting Li^+ ions during the charge and discharge cycle (topotactic adsorption/intercalation). 2H-MoS_2, a potential alternative anode material to graphite, undergoes a phase transition when interspersed with a large amount of Li [12]. This phase transition occurs due to the large charge transfer from Li to 2H-MoS_2, resulting in a loss of energy in the battery cycle. To analyze the structural stability of NbS_2, we first studied the difference between the total energies of the 2H and 1T phases as a function of the net electrical charge of the system. For a neutral material, the 2H phase is more energetically favorable than the 1T phase by $\Delta E = -0.13$ eV per unit cell. Upon donating electrons to the system (negative net charge), the energy difference decreases linearly until $\Delta E = -0.41$ eV at an electronic density of $n = 10^{15}$ cm^{-2}. Removing electrons from the system (positive net charge) causes the energy difference ΔE to increase linearly until reaching $\Delta E = 0$ at $p_c = 4 \times 10^{14}$ cm^{-2} or up to $\Delta E = +0.18$ eV for the hole density $p = 10^{15}$ cm^{-2} (Figure 2A). Variations of these total energies for each phase indicate that the phase transition from 2H to 1T may only occur when the material is doped with positive charge carriers (holes) or when acceptor impurities are adsorbed.

Although the differences in total energy are indicative of phase transitions, a more detailed study can be done by simulating the TS using the NEB method (see the Section 2). Calculating these phase transitions with the charged materials revealed a variation in barrier height between the 2H and 1T phases with net charge. In contrast, for the neutral material, the height of the energy barrier is $\Delta E^{\ddagger} = 0.58$ eV per unit cell, which decreases to $\Delta E^{\ddagger} = 0.16$ eV when the hole density $p = 10^{15}$ cm^{-2}. Even with the difference in total energy, which is favorable for the phase transition at $p = 10^{15}$ cm^{-2}, there is still an overlap in energy barrier, as shown in Figure 2B. For negatively charged materials, the barrier heights only increase with electron density. Snapshots of the phase transition calculated using the NEB method are shown in Figure 2D. Note that there are asynchronous displacements among the S atoms in one of the NbS_2 sublayers, as indicated by black arrows in Figure 2D. In the NEB calculation with a primitive unit cell, the energy barrier is greater due to the symmetry constraint maintained in the phase transition, as shown in Figure S2. In addition to studying the energy barriers as a function of net charge, we also simulated the TSs of NbS_2 with adsorbed Li^+. Figure 2C shows the energy barriers with Li^+ adsorption. The shift in the sulfur atomic plane can occur on the same side as Li^+ adsorption (top) or on the opposite side of Li^+ adsorption (bottom). For each of these two configurations, Li^+ can also be adsorbed at the M and h sites. All these four phase transition scenarios have higher energy barriers than the pristine system. As Li atoms donate electrons to NbS_2, the material becomes negatively charged, and the energy barriers increase. This increase in energy barrier demonstrates the structural stability of NbS_2 with Li^+ adsorption, which is opposite the behavior observed in 2H-MoS_2.

3.3 | Charge transfer

Charge transfer is an important chemical property for storing energy in battery electrodes. When Li is adsorbed in the basal plane of NbS_2, charge transfer occurs from Li to the 2D material. This charge transfer shifts the Fermi level of the 2D material and changes the shape of the density of states. To study this charge transfer, we calculated the projected density of states (PDOS) for pristine 2H-NbS_2 and 2H-NbS_2 with three proportions of Li coverage on the basal plane: 13%, 50%, and 100% (Figure 3A). In Figure 3A, Nb states are represented by the light blue area, while Li states are represented by the red area. In all these cases, NbS_2 remained metallic with electrical conduction via the basal plane. The PDOS for 1T-NbS_2 with Li adsorption are depicted in Figure S3. In fact, both the 2H and 1T phases of NbS_2 are metallic for all Li coverage percentages.

The partial charges for each atom of the unit cell in pristine NbS_2 and NbS_2 with adsorbed Li were calculated using Bader analysis. For pristine NbS_2, Nb is a cation with partial charge $q = +2$ |e|, and S is an anion with partial charge $q = -1$ |e| [Figure 3B]. With the adsorption, the Li atom completely loses the 2 *s* electron and becomes a cation with charge $q = +1$ |e|. The electron donation occurs mainly for the S atom closest to Li (S_{up}) and in a smaller proportion for Nb. Meanwhile, the partial charge of the S atom below Nb (S_{down}) remains virtually unchanged. This charge transfer can also be seen by the difference in density:

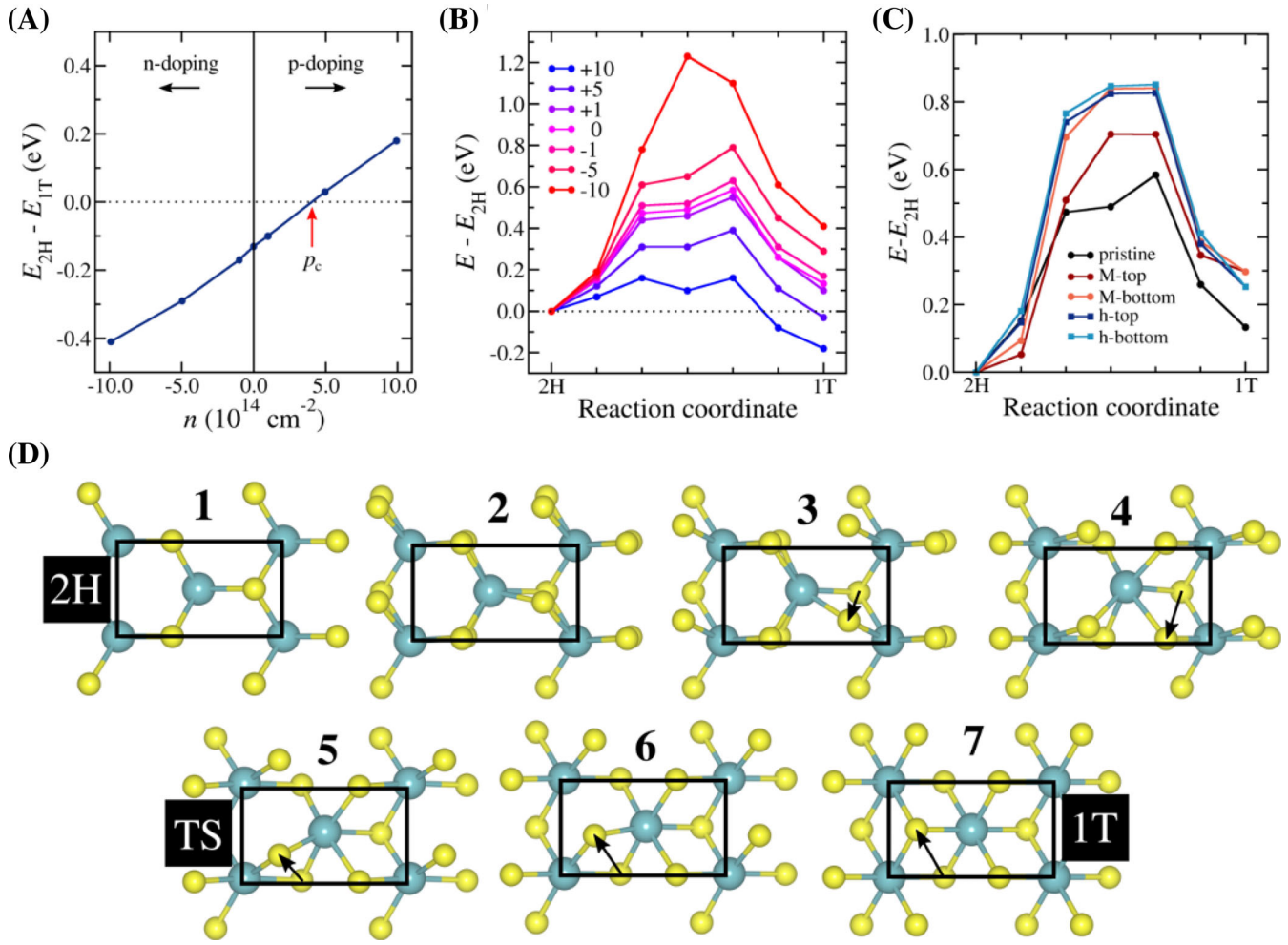

FIGURE 2 NbS_2 phase transition. (A) Difference in energy between the 2H and 1T phases as a function of net electron density. (B) Energy barrier diagrams of the NbS_2 phase transition for various values of electron density (10^{14} cm^{-2}). (C) Energy barrier diagrams for the phase transition of Li-doped NbS_2. (D) Snapshots of the nudged elastic band (NEB) unit cell from simulation of the NbS_2 phase transition

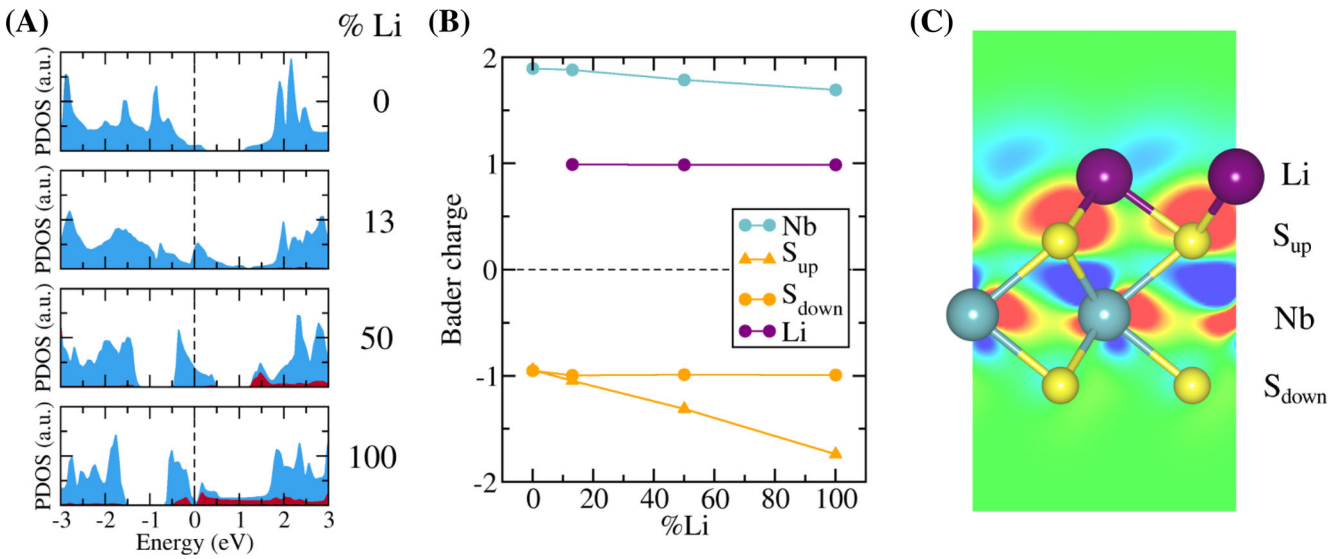

FIGURE 3 Li_xNbS_2 charge transfer. (A) Projected density of states (PDOS) of Li_xNbS_2 for x = 0, 0.13, 0.5, and 1.0. NbS_2 states are shown in blue, whereas Li states are shown in red. The Fermi level (black dashed line) is set to zero. (B) Bader charge analysis for Li_xNbS_2. (C) Volume slice plot of the charge difference $\Delta\rho$. Accumulation (depletion) of electrons is shown in red (blue)

$$\Delta\rho = \rho_{Li_xNbS_2} - \rho_{NbS_2} - \rho_{Li_x}, \tag{2}$$

as shown in Figure 3C, where the accumulation (depletion) of electrons is shown in red (blue), while regions with no change in charge density are shown in green.

Making use of the partial charge of Li, we can estimate the specific capacity by the Faraday's equation:

$$C = \frac{xzF}{M_{NbS_2}}, \tag{3}$$

where F = 26.801 Ah/mol is the Faraday constant, z is the charge transferred from the ion to the anode, x is the fraction of Li ions per NbS_2 formula, and M_{NbS_2} is the NbS_2 molar mass. The highest capacity obtained in this work was C = 341 mAh/g. Although these specific capacities are relatively low, recent strategies with TMD frameworks can significantly increase these values to up to 700 mAh/g [8].

3.4 | Lithium diffusion

The fast diffusion of Li^+ cations is one of the essential criteria of a high-performance LIB. To calculate the diffusion kinetics of Li adsorbed on NbS_2, we simulated the TSs of Li^+ cations transiting at equivalent adsorption sites. Figure 4A shows a ball-and-stick representation of a snapshot from the TS calculation performed with the NEB method. The corresponding energy barrier diagrams are shown in Figure 4B. The energy barrier for low Li coverage (13%) is $\Delta E^{\ddagger}$ = 0.12 eV, while that for high Li coverage (100%) is increased to $\Delta E^{\ddagger}$ = 0.24 eV. For comparison, the energy barrier for the diffusion of Li^+ on 2H-MoS_2 is 0.19 eV for low Li coverage (13%). The small energy barrier in the case of low Li coverage results in a high diffusivity of Li^+ in NbS_2.

The diffusivity is calculated as a function of temperature by

$$D(T) = \lambda^2 k_{TS}, \tag{4}$$

where λ = 3.362 Å is the distance from equivalent Li adsorption sites, and k_{TS} is the kinetic rate constant for diffusion given by the Eyring's equation [27]:

$$k_{TS} = \frac{k_B T}{h}\exp\left(-\frac{\Delta E^{\ddagger}}{k_B T}\right), \tag{5}$$

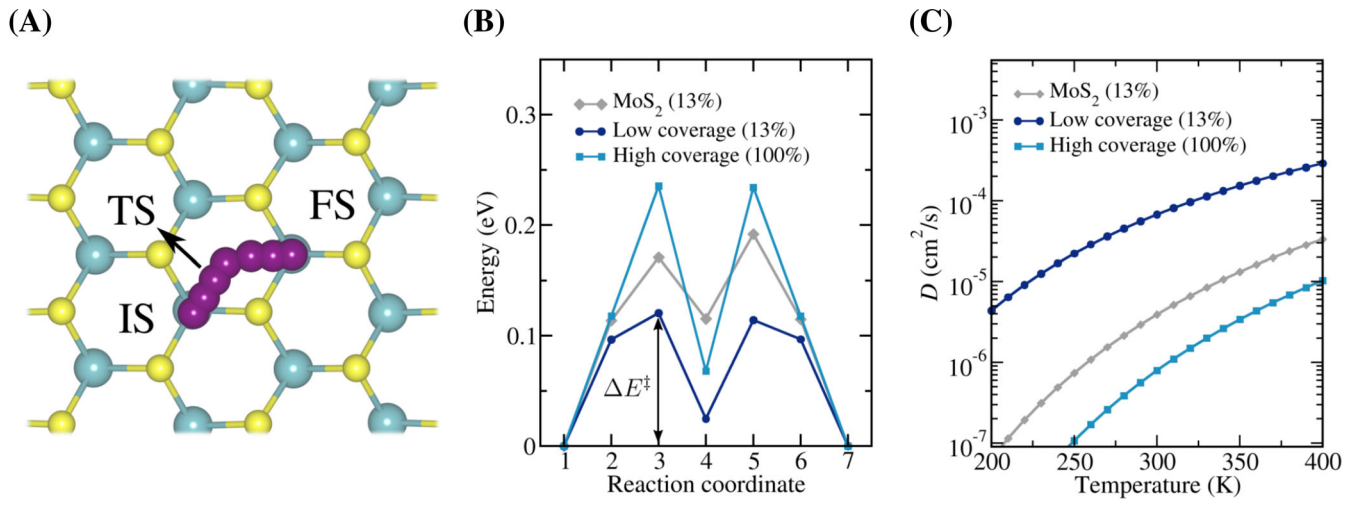

FIGURE 4 Lithium diffusion on 2H-NbS_2. (A) Ball-and-stick representation of Li^+ diffusion on NbS_2 based on the nudged elastic band (NEB) method. (B) Energy barrier diagram for Li^+ diffusion for low (13%) and high (100%) Li coverages on NbS_2. (C) Diffusion coefficients for low and high Li coverages as functions of temperature. The calculated data for 2H-MoS_2 are shown as a reference

where k_B is the Boltzmann constant, T is the temperature, h is Planck's constant, and $\Delta E^{\ddagger}$ is the energy barrier height (activation energy) shown in Figure 4B. The diffusivities for low and high Li coverages are shown in Figure 4C. For low Li coverage (13%) at room temperature (300 K), the diffusivity is $D = 6 \times 10^{-5}$ cm^2/s, ~17 times faster than the diffusion of Li^+ on 2H-MoS_2. This ultrafast diffusion is similar to the diffusion of Li^+ between layers of graphene [28, 29]. This high Li^+ diffusivity is explained by the small difference in adsorption energy between the M and h sites in NbS_2 (Figures 1C and S1) since the M site is the initial and final state, and the h site is an intermediate state. The differences between the adsorption energies of the M and h sites are greater in MoS_2 than in NbS_2, which explains the greater energy barrier and lower diffusion coefficient of MoS_2.

4 | CONCLUSIONS

Based on first-principles simulations, we have shown that 2H-NbS_2 monolayer meets the important criteria of new anode materials for LIBs. 2H-NbS_2 monolayer exhibits high structural stability upon Li adsorption and, unlike 2H-MoS_2, does not undergo a phase transition to the 1T phase upon electron doping. Since both the 2H and 1T phases of NbS_2 are metallic, a phase transition is not necessary to increase the electrical conductivity of the material. The high adhesion of Li^+ cations to NbS_2 reduces the tendency to form Li dendrites on the electrode during the recharging process. Both 2H-NbS_2 and 1T-NbS_2 are metallic from their pristine forms up to high coverages of Li. Li^+ cations adsorbed on 2H-NbS_2 diffuse in a ultrafast way on the basal plane, with diffusivity reaching $D = 6 \times 10^{-5}$ cm^2/s at room temperature. These outstanding physical properties make 2H-NbS_2 monolayer as a potential candidate for replacing graphite as the negative electrode material in LIBs.

ACKNOWLEDGMENTS

We thank Prof. Camila M. Maroneze and Prof. Cecília C. Castro e Silva for valuable discussions about the manuscript.

AUTHOR CONTRIBUTIONS

Armando de Rezende Neto: Investigation. **Leandro Seixas:** Conceptualization; funding acquisition; methodology; project administration.

RESEARCH RESOURCES

We thank the High Performance Computing Center (NACAD) at COPPE/UFRJ for providing computational facilities.

ORCID

Leandro Seixas https://orcid.org/0000-0001-7420-0708

REFERENCES

[1] H. Li, Z. Wang, L. Chen, X. Huang, *Adv. Mater.* **2009**, *21*(45), 4593.
[2] N. Nitta, F. Wu, J. T. Lee, G. Yushin, *Mater. Today* **2015**, *18*(5), 252.
[3] The nobel prize in chemistry; 2019. NobelPrize.org.
[4] W. Li, Y. Yang, G. Zhang, Y.-W. Zhang, *Nano Lett.* **2015**, *15*(3), 1691.
[5] S. Karmakar, C. Chowdhury, A. Datta, *J. Phys. Chem. C* **2016**, *120*(27), 14522.
[6] Q. Sun, Y. Dai, Y. Ma, T. Jing, W. Wei, B. Huang, *J. Phys. Chem. Lett.* **2016**, *7*(6), 937.
[7] G. Du, Z. Guo, S. Wang, R. Zeng, Z. Chen, H. Liu, *Chem. Commun.* **2010**, *46*(7), 1106.
[8] H. Hwang, H. Kim, J. Cho, *Nano Lett.* **2011**, *11*(11), 4826.
[9] D. Wang, Y. Liu, X. Meng, Y. Wei, Y. Zhao, Q. Pang, G. Chen, *J. Mater. Chem. A* **2017**, *5*(40), 21370.
[10] C. Feng, J. Ma, H. Li, R. Zeng, Z. Guo, H. Liu, *Mater. Res. Bull.* **2009**, *44*(9), 1811.
[11] Q. Wang, J. Li, *J. Phys. Chem. C* **2007**, *111*(4), 1675.
[12] D. Nasr Esfahani, O. Leenaerts, H. Sahin, B. Partoens, F. Peeters, *J. Phys. Chem. C* **2015**, *119*(19), 10602.
[13] K. F. Mak, C. Lee, J. Hone, J. Shan, T. F. Heinz, *Phys. Rev. Lett.* **2010**, *105*(13), 136805.
[14] J. Zhang, C. Du, Z. Dai, W. Chen, Y. Zheng, B. Li, Y. Zong, X. Wang, J. Zhu, Q. Yan, *ACS Nano* **2017**, *11*(10), 10599.
[15] E. Yang, H. Ji, Y. Jung, *J. Phys. Chem. C* **2015**, *119*(47), 26374.
[16] P. Hohenberg, W. Kohn, *Phys. Rev.* **1964**, *136*(3B), B864.
[17] W. Kohn, L. J. Sham, *Phys. Rev.* **1965**, *140*(4A), A1133.
[18] A. García, N. Papior, A. Akhtar, E. Artacho, V. Blum, E. Bosoni, P. Brandimarte, M. Brandbyge, J. Cerdá, F. Corsetti, R. Cuadrado, V. Dikan, J. Ferrer, J. Gale, P. García-Fernández, V. M. García-Suárez, S. García, G. Huhs, S. Illera, R. Korytár, P. Koval, I. Lebedeva, L. Lin, P. López-Tarifa, S. G. Mayo, S. Mohr, P. Ordejón, A. Postnikov, Y. Pouillon, M. Pruneda, R. Robles, D. Sánchez-Portal, J. M. Soler, R. Ullah, V. W.-Z. Yu, J. Junquera, *J. Chem. Phys.* **2020**, *152*(20), 204108.
[19] N. Troullier, J. L. Martins, *Phys. Rev. B* **1991**, *43*(3), 1993.
[20] J. Perdew, K. Burke, M. Ernzerhof, *Phys. Rev. Lett.* **1996**, *77*(18), 3865.
[21] H. J. Monkhorst, J. D. Pack, *Phys. Rev. B* **1976**, *13*(12), 5188.
[22] G. Henkelman, H. Jónsson, *J. Chem. Phys.* **2000**, *113*(22), 9978.

[23] A. H. Larsen, J. J. Mortensen, J. Blomqvist, I. E. Castelli, R. Christensen, M. Dułak, J. Friis, M. N. Groves, B. Hammer, C. Hargus, E. D. Hermes, P. C. Jennings, P. B. Jensen, J. Kermode, J. R. Kitchin, E. L. Kolsbjerg, J. Kubal, K. Kaasbjerg, S. Lysgaard, J. B. Maronsson, T. Maxson, T. Olsen, L. Pastewka, A. Peterson, C. Rostgaard, J. Schiøtz, O. Schütt, M. Strange, K. S. Thygesen, T. Vegge, L. Vilhelmsen, M. Walter, Z. Zeng, K. W. Jacobsen, *J. Phys. Condens. Matter* **2017**, *29*(27), 273002.
[24] V. V. Kulish, O. I. Malyi, C. Persson, P. Wu, *Phys. Chem. Chem. Phys.* **2015**, *17*(21), 13921.
[25] S. Mukherjee, L. Kavalsky, C. V. Singh, *ACS Appl. Mater. Interfaces* **2018**, *10*(10), 8630.
[26] T. Wang, R. V. Salvatierra, J. M. Tour, *Adv. Mater.* **2019**, *31*(14), 1807405.
[27] H. Eyring, *J. Chem. Phys.* **1935**, *3*(2), 107.
[28] M. Kühne, F. Paolucci, J. Popovic, P. M. Ostrovsky, J. Maier, J. H. Smet, *Nat. Nanotechnol.* **2017**, *12*(9), 895.
[29] K. Zhong, R. Hu, G. Xu, Y. Yang, J.-M. Zhang, Z. Huang, *Phys. Rev. B* **2019**, *99*(15), 155403.

SUPPORTING INFORMATION

Additional supporting information may be found online in the Supporting Information section at the end of this article.

How to cite this article: de Rezende Neto AS, Seixas L. Toward a two-dimensional NbS_2-based electrode for lithium–ion batteries. *Int J Quantum Chem*. 2021;e26603. https://doi.org/10.1002/qua.26603